Dual-polarized Dual-band Mobile 5G Antenna Array

Igor Syrytsin, Shuai Zhang and Gert F. Pedersen
Department of Electronic Systems, Aalborg University, Fredrik Bajers Vej 7, Aalborg, Denmark

Keywords: Antenna Array, 5G Antenna, Dual-band, Dual-polarized Antenna, Phased Array.

Abstract: In this paper, a dual-band dual-polarized phased antenna array for 5G mobile terminals is proposed. The array has a bandwidth of 3.6 GHz and two resonances at 30.5 and 32.8 GHz. The array has a clearance of 2.85 mm and fed with two ports in simulation to excite the notch and dipole parts of the proposed antenna structure. Finally, the proposed antenna element is combined into two arrays with different configurations. It is shown that it is better to use the array of 8 elements than to use two 4-element sub-arrays with orthogonal orientation.

1 INTRODUCTION

In the recent years the research community and the industry has been working towards standardization of 5G mm-wave communication system. Because the bandwidth is a scarce resource at the current frequency bands under 6 GHz it is decided to implement the 5G mm-wave system in the mm-wave frequency spectrum (Rappaport et al. 2013). Currently, eleven candidate bands in the range between 24.25 GHz and 86 GHz have been considered for the 5G mm-wave communication system (Lee et al. 2018). To combat the high path loss expected at the mm-wave frequencies antennas with the gain higher than 7 dBi at both mobile and base stations. However, because the orientation of the mobile terminal is not known, beamforming will be implemented in order to achieve spatial coverage requirements (Roh et al. 2014). The spatial performance of the mobile terminal can be characterized by using the metric of coverage efficiency, which has been first proposed in (Rehman et al. 2012) and then applied to 5G mobile terminal antennas in (Helander et al. 2016). Furthermore, in (Nielsen & Pedersen 2016) it has been shown that in the typical indoor propagation channel the received power depends strongly on the polarization of transmitter and receiver antennas. The measurements has shown that up to 10 dB difference can be seen between different antenna polarization combinations, but the co-polarized antenna configurations are not always the best option for the indoor channel. Thus, a polarization reconfigurable antenna is required to adapt to the channel changes and keep the received power at the highest possible level.

Antenna array with multiple polarizations is proposed in (Hong et al. 2015) for the mm-Wave 5G mobile terminals. Then, a low-profile antenna solution with beam-steering capabilities is proposed in in (Hong et al. 2014). A Vivaldi phased antenna array performance and it's user effects are investigated in (Ojaroudiparchin et al. 2015). In (Hussain et al. 2017) a compact 4G MIMO antenna is integrated with the 5G mm-wave mobile array. Two different methods in (Ojaroudiparchin et al. 2016) and (Zhang et al. 2017) are introduced in order to create a 3D coverage 5G mm-wave phased antenna array system. Three sub-arrays mounted on the folded 3D structure are constructed in (Ojaroudiparchin et al. 2016). Then, in (Zhang et al. 2017) a surface wave is efficiently utilized to change the radiation direction of slot array elements. However, for 5G mm-wave a bandwidth of at least 1.6 GHz is required. The wideband antenna array for 5G mobile terminals has been presented in (Syrytsin et al. 2018). The proposed antenna element utilizes four modes in order to achieve the wideband performance. Circular polarized antennas has been proposed in (Mahmoud & Montaser 2018), (Syrytsin et al. 2017) and (Shuai Zhang 2018). Furthermore, polarization reconfigurability and small clearance are also very important design considerations for 5G mobile antennas.

In this work, a dual-band dual-polarized 5G mobile phased antenna array is presented. The proposed antenna consists of two co-located antennas which can operate at the same frequency but radiate with orthogonal polarizations. The antenna structure is designed for the 5G frequency band of 30.8 to 33.4 GHz. However, because the 5G frequency bands are not finally defined yet, it has been chosen to increase the bandwidth of the antenna by introducing a second res-

Syrytsin, I., Zhang, S. and Pedersen, G.
Dual-polarized Dual-band Mobile 5G Antenna Array.
DOI: 10.5220/0006919403090315
In *Proceedings of the 15th International Joint Conference on e-Business and Telecommunications (ICETE 2018) - Volume 1: DCNET, ICE-B, OPTICS, SIGMAP and WINSYS*, pages 309-315
ISBN: 978-989-758-319-3

onance. A bandwidth of 3.6 GHz is achieved by both antennas with the ground plane clearance of 2.85 mm. The antenna structure can be easily tuned to other frequency range by changing a number of antenna structure dimensions. Finally, the performance of the phased array in two configurations has been investigated. The metrics of the total scan pattern and coverage efficiency have been used to quantify the simulation results.

2 ANTENNA ELEMENT PERFORMANCE

In this section, the geometry, operation principle, performance and design considerations of the proposed antenna element will be described. Surface currents, reflection coefficient and radiation patterns are used to describe the performance of the antenna element.

2.1 Antenna Geometry

The geometry of the proposed antenna element is shown in Figure 1. The antenna is built on the Rogeres RO4350B substrate with a thickness of 0.762 mm. As shown in Figure 1, the dual polarized antenna element consists of two parts. In simulation setup, the dipole part is fed by the port P1, which is located between the two dipole arms. The other port is located between the top and bottom layer of the PCB. The port 2 (P2) induces the currents on the top and bottom rings around the patch in the middle, and thus produce the radiation. In Figure 1 the constant geometry dimensions are shown as numbers, and variable dimensions are displayed in words. The variable dimensions can be altered in order to change the resonant frequency of the antenna modes.

2.2 Antenna Operation Principle

The reflection coefficients at the ports 1 and 2 are shown in Figure 2 and denoted as s-parameters S11 and S22. It can be noticed that two resonances appear when the antenna structure is fed at either port 1 or port 2. A resonance frequency of the first mode is around 30.5 GHz and around 32.8 GHz for the second mode. Furthermore, in Figure 2 a band from 31.8 to 33.5 GHz is visualized in a gray color.

To grasp the operation principle of the proposed antenna it has been chosen to show the maximum surface currents on the antenna structure in Figure 3. The substrate and the bottom layer are hidden. Notice the orientation of Z-axes in the figure, which is pointing outside of the paper. From both figures it is clear that

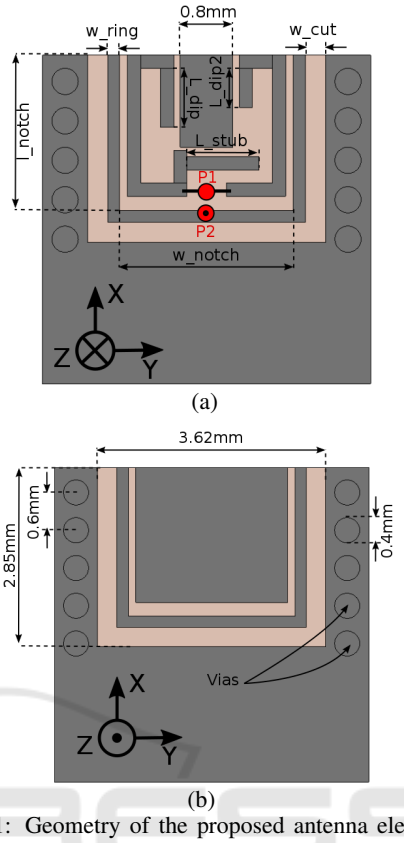

Figure 1: Geometry of the proposed antenna element (a) front view, (b) back view.

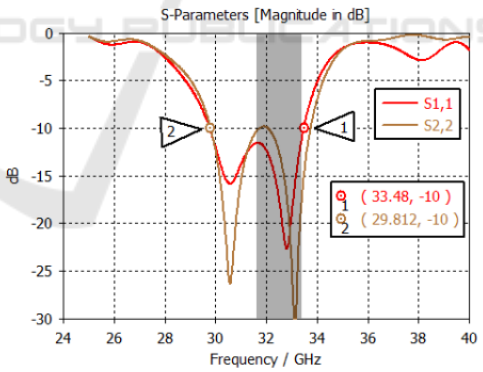

Figure 2: Reflection coefficients at the port 1 and port 2.

the vias can efficiently reduce the surface wave on the ground plane. The dipole is excited by the port 1 in Figure 3(a) at 30.5 GHz and in Figure 3(a) at 32.8 GHz. It can clearly be seen that in mode 1 the radiation is created by the left dipole arm, and mode 2 is created by the currents running on the right dipole arm and stub. In comparison to the dipole modes, the modes of the rings induce higher currents on the ground plane in Figure 3(c) and Figure 3(d). When port 2 is excited at 30.5 GHz then the highest currents are concentrated on the ring (left and right side).

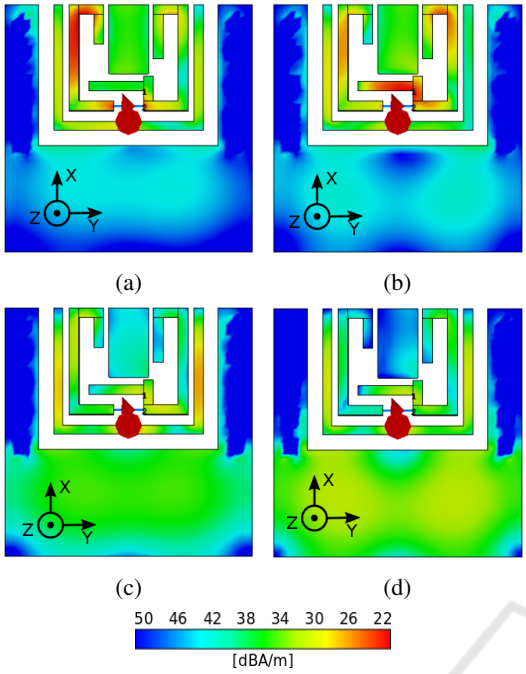

Figure 3: Maximum surface currents on the antenna structure produced by the (a) port 1 – mode 1, (b) port 1 – mode 2, (c) port 2 – mode 1, and (d) port 2 – mode 2.

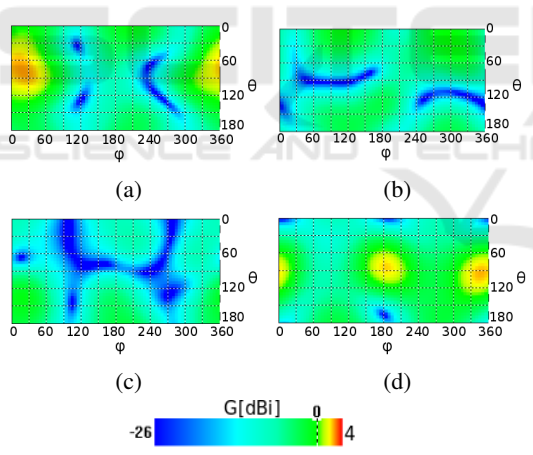

Figure 4: Radiation pattern of the proposed antenna structure excited at (a) port 1 - yz-polarization, (b) port 1 - xz-polarization, (c) port 2 - yz-polarization, and (d) port 2 - xz-polarization.

However, when port 2 is excited at 32.8 GHz, then the currents are equally distributed among the ring and ground plane. Furthermore, the patch in the middle, between dipole arms, is added to tune the impedance matching of a dipole. Thus, the patch is not excited when the ring is radiating instead of the dipole.

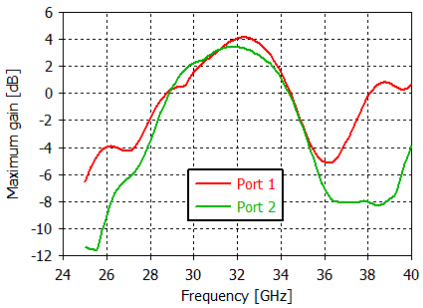

Figure 5: Realized gain over the frequency range of the proposed antenna.

2.3 Antenna Performance

Next, it has been chosen to show radiation patterns of the antenna structure excited with port 1 and port 2. Here, two distinct polarizations are defined: xz-polarization and yz-polarization. The radiation pattern of the proposed antenna structure is shown in Figure 4. It can clearly be seen that the dipole antenna structure has yz-polarization, as shown in Figure 4(a). When the structure is excited by the port 1 the xz component of the antenna gain is very low in Figure 4(b). However, for when the structure is excited by the port 2 the xz component of the antenna gain has a highest value in Figure 4(d).

Next, the maximum gain over the frequency range from 24 to 40 GHz is shown in Figure 5. The realized gain in the band of interest is higher than 2 dBi when the antenna structure is excited by either port 1 or 2.

2.4 Dipole Design

In this section, it will be shown how to control the resonance behavior of the dipole part of the proposed antenna structure (when the structure is excited by the port 1). The parametric results for the reflection coefficient at port1 are shown in Figure 6 for the three different antenna structure parameters defined in Figure 1. First, the length of one of the dipole arms l_{dip} is changed from 0.4 to 1.1 mm as shown in Figure 6(a). It can be seen that by changing that parameter the matching of both modes is changing, but the resonance frequency of modes remains the same. Next, in Figure 6(b) the length of another dipole arm is swept from 0.1 to 1.1 mm. Here more severe effect on the resonance 1 is observed, but resonance frequency of mode 2 remains the same. Finally, the length of the stub is swept from 0.5 to 1 mm. Now the resonance frequency of mode 2 changes significantly, while the resonance frequency of the mode 1 is unchanged. To move the antenna resonances one should first change the resonance of mode 1 by changing the length l_{dip2}

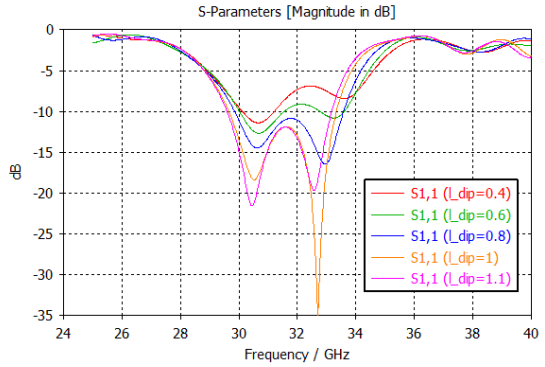

(a)

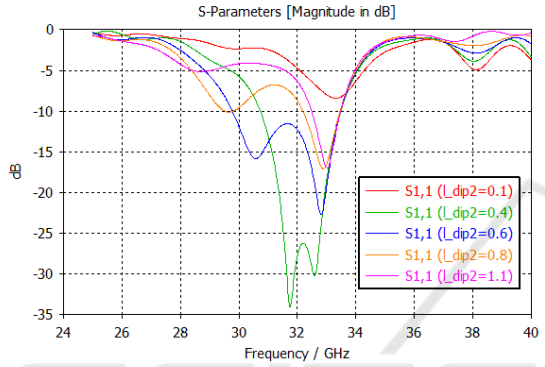

(b)

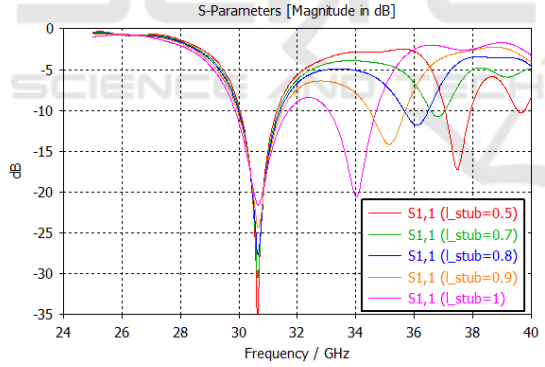

(c)

Figure 6: Parametric results of the reflection coefficient when lengths (a) l_{dip}, (b) l_{dip2}, and (c) l_{stub} are permuted.

, then change the resonance of mode 2 by tuning the length of stub l_{stub}, and finally match the antenna according to the specifications by tuning the parameter l_{dip}.

2.5 Notch Design

In this subsection it will be shown how to control the resonance behavior of the notch part of the antenna structure (when the antenna structure is excited by the port 2). The corresponding antenna structure parameters are defined in Figure 1. To tune the resonance frequencies of notch modes it has been chosen to show the effect of changing the values of four parameters of the antenna structure which is shown in Figure 7. First, it can be noticed that a single parameter cannot be used to change the matching of the antenna. The resonance frequency of the modes always shifts, so multiple notch parameters need to be adjusted in order to change the matching of the antenna. To change the resonance frequency of mode 2 the parameter l_{notch} and w_{notch} should be permuted in Figure 7(a) and Figure 7(b). However, if the resonance frequency of mode 1 is to be altered, then the parameters w_{ring}, w_{cut}, and w_{notch} should be permuted. It can be already noticed that the design of the notch part of the antenna is more complicated and not so straightforward as the dipole design.

3 PERFORMANCE OF THE PHASE ARRAY

In this section, the performance of the mm-wave phased array constructed by using the proposed dual-polarized antenna element will be investigated. To investigate the performance of the array the metrics of the total scan pattern and coverage efficiency are used. The coverage efficiency is calculated from the total scan pattern (TSP) of the phased array or switchable antenna array system and obtained from all antenna array patterns, corresponding to the different scan angles. The best achievable gain is extracted at every spatial point.

The coverage efficiency is defined as (Helander et al. (2016)):

$$\eta_c = \frac{\text{Coverage Solid Angle}}{\text{Maximum Solid Angle}} \quad (1)$$

where the maximum solid angle defined as 4π steradians. The coverage efficiency has no unit and varies from 0 to 1 (corresponding to 0 and 100 % coverage).

3.1 Array Geometry

In this paper, it has been chosen to investigate the performance of the proposed antenna element in the linear arrays in two configurations. The two array configurations are shown in Figure 8. In the configuration 1 in Figure 8(a) 8 elements are distributed into two sub-arrays of four elements, perpendicular to each other. And in the configuration 2 in Figure 8(b) 8 same elements are combined into one linear array of 8 elements. The point is to investigate which configuration has better performance. From the system point

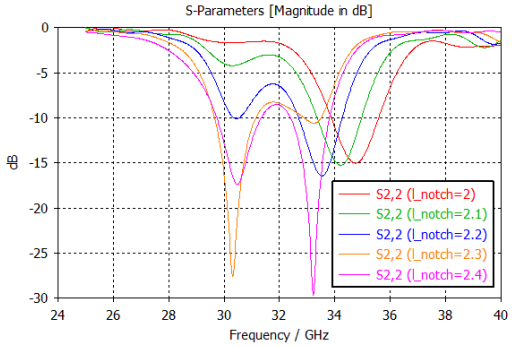

(a)

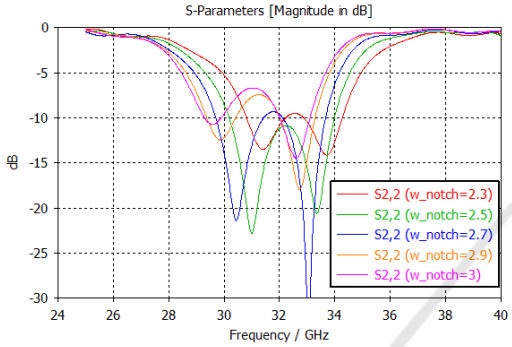

(b)

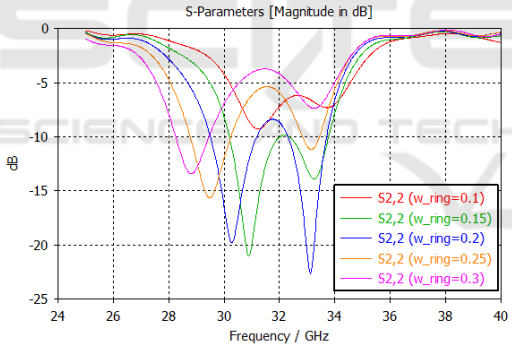

(c)

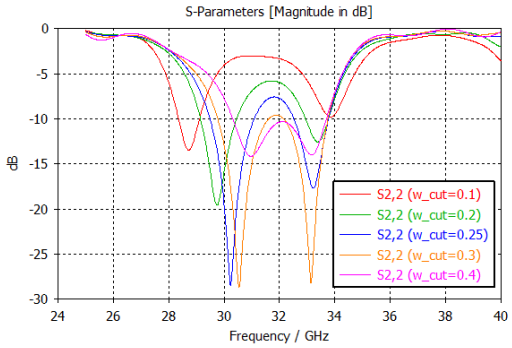

(d)

Figure 7: Parametric results of the reflection coefficient when lengths (a) l_{notch}, (b) w_{notch}, (c) w_{ring}, and (d) w_{cut} are permuted.

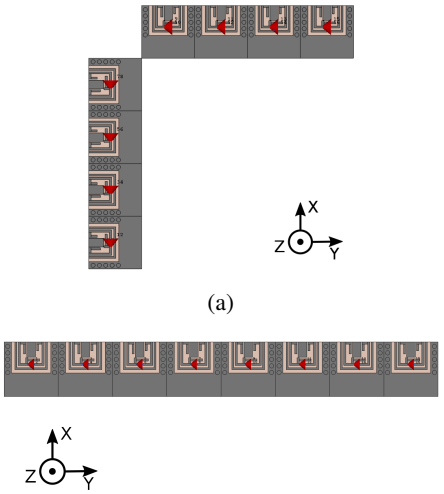

(a)

(b)

Figure 8: Two configurations of the phased antenna array (a) two sub-arrays of four elements and (b) one 8-element phased array.

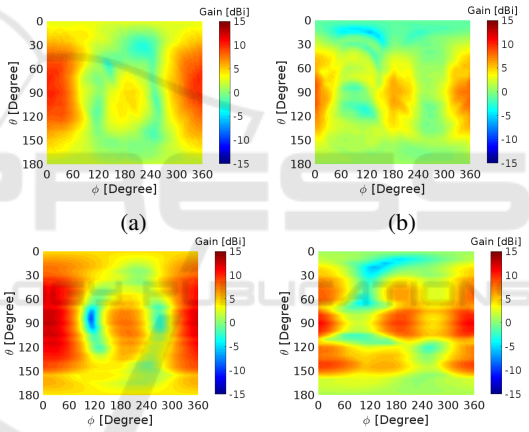

(a) (b) (c) (d)

Figure 9: Total scan patterns of (a) configuration 1 – xz polarization, (b) configuration 1 – yz polarization, (c) configuration 2 – xz polarization, and (d) configuration 2 – yz polarization.

of view, the configuration 1 requires less complicated feeding network and SPDT switch. Where the configuration 2 requires more complicated feeding network but no switch. Furthermore, the sub-arrays in the configuration 1 is oriented perpendicular to each other in order to maximize the coverage (scanning in xz and yz-planes). On the other hand, the phased array in the configuration 2 can only scan in yz-plane.

The total scan patterns of the two proposed phased antenna array configurations at 32 GHz are shown in Fig. 9. It can be seen that the maximum gain in the configuration 1 in lower than the maximum gain in the configuration 2. However, side lobes are higher in the case of configuration 2 in Figure 9(d).

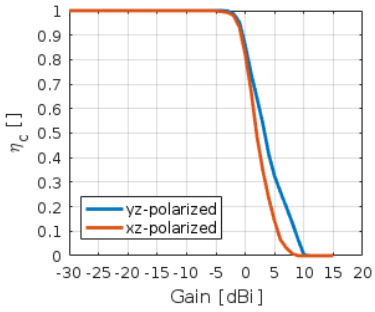

(a)

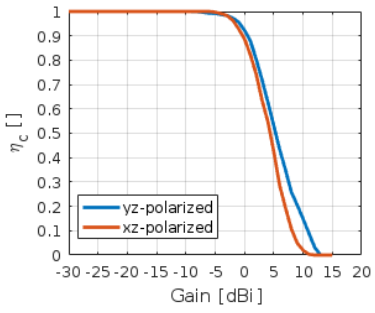

(b)

Figure 10: Coverage efficiency of phased antenna array in (a) configuration 1 and (b) configuration 2.

Finally, the coverage efficiency of the array in two configurations is calculated and shown in Figure 10. First, it can be noticed that difference in the coverage between two polarization is very small for the gains lower than 0 dBi. However, a bigger difference can be seen as the gain increases. Finally, the curves for the array configuration 1 and configuration 2 have a very similar slope, but the absolute level of the coverage is different. It can be seen that the array in the configuration 1 have 20 % less coverage for the gain of 5 dBi.

4 CONCLUSION

In this paper, a dual-polarized dual-band phased antenna array for 5G mobile devices has been presented. The proposed array have the bandwidth of 3.6 GHz and covers the band of 30.8 to 33.4 GHz. Furthermore, it has been shown how to tune each mode of the antenna in order to achieve the desired bandwidth and resonance frequency of each mode. Next, two phased array configurations have been investigated. One configuration has 8 array elements distributed into two 4-element sub-arrays oriented orthogonally with respect to each other. It has been found that array of 8 elements give better spatial coverage performance. However, this investigation has only been done for the broadside antenna element. A further investigation of endfire antenna element should also be conducted in the future work.

REFERENCES

Helander, J., Zhao, K., Ying, Z. & Sjöberg, D. (2016), 'Performance analysis of millimeter-wave phased array antennas in cellular handsets', *IEEE Antenna Wireless Propagation Letters* **15**, 504–507.

Hong, W., Baek, K., Lee, Y. & Kim, Y. G. (2014), 'Design and analysis of a low-profile 28 GHz beam steering antenna solution for Future 5G cellular applications', *Microwave Symposium (IMS), 2014 IEEE MTT-S International* pp. 1–4.

Hong, W., Ko, S. T., Lee, Y. & Baek, K. H. (2015), 'Multipolarized antenna array configuration for mmWave 5G mobile terminals', *2015 International Workshop on Antenna Technology (iWAT)* pp. 60–61.

Hussain, R., Alreshaid, A. T., Podilchak, S. K. & Sharawi, M. S. (2017), 'Compact 4G MIMO antenna integrated with a 5G array for current and future mobile handsets', *IET Microwaves, Antennas & Propagation* **11**(2), 271–279.

Lee, J., Tejedor, E., Ranta-aho, K., Wang, H., Lee, K. T., Semaan, E., Mohyeldin, E., Song, J., Bergljung, C. & Jung, S. (2018), 'Spectrum for 5g: Global status, challenges, and enabling technologies', *IEEE Communication Magazine* **56**(3), 12–18.

Mahmoud, K. R. & Montaser, A. M. (2018), 'Design of dual-band circularly polarised array antenna package for 5G mobile terminals with beam-steering capabilities', *IET Microwaves, Antennas Propagation* **12**(1), 29–39.

Nielsen, J. O. & Pedersen, G. F. (2016), Dual-polarized indoor propagation at 26 ghz, *in* '2016 IEEE 27th Annual International Symposium on Personal, Indoor, and Mobile Radio Communications (PIMRC)', pp. 1–6.

Ojaroudiparchin, N., Shen, M. & Pedersen, G. F. (2015), 'Design of Vivaldi antenna array with end-fire beam steering function for 5G mobile terminals', *2015 23rd Telecommunications Forum Telfor (TELFOR)* pp. 587–590.

Ojaroudiparchin, N., Shen, M., Zhang, S. & Pedersen, G. F. (2016), 'A Switchable 3-D-Coverage-Phased Array Antenna Package for 5G Mobile Terminals', *IEEE Antennas Wireless Propagation Letters* **15**, 1747–1750.

Rappaport, T. S., Sun, S., Mayzus, R., Zhao, H., Azar, Y., Wang, K., Wong, G. N., Schulz, J. K., Samimi, M. & Gutierrez, F. (2013), 'Millimeter wave mobile communications for 5G cellular: It will work!', *IEEE Access* **1**, 335–349.

Rehman, M. U., Chen, X., Parini, C. G. & Ying, Z. (2012), 'Evaluation of a statistical model for the characterization of multipath affecting mobile terminal GPS antennas in sub-urban areas', *IEEE Transactions on Antennas and Propagation* **60**(2), 1084–1094.

Roh, W., Seol, J. Y., Park, J., Lee, B., Lee, J., Kim, Y., Cho, J., Cheun, K. & Aryanfar, F. (2014), 'Millimeter-wave beamforming as an enabling technology for 5G cellular communications: theoretical feasibility and prototype results', *IEEE Communication Magazine* **52**(2), 106–113.

Shuai Zhang, Igor Syrytsin, G. F. P. (2018), Substrate-insensitive phased array with improved circularly-polarized scan angle for 5G mobile terminals, *in* 'EuCAP 2018, the 12th European Conference on Antennas and Propagation'.

Syrytsin, I., Zhang, S. & Pedersen, G. F. (2017), Circularly polarized planar helix phased antenna array for 5g mobile terminals, *in* '2017 International Conference on Electromagnetics in Advanced Applications (ICEAA)', pp. 1105–1108.

Syrytsin, I., Zhang, S., Pedersen, G. F. & Morris, A. (2018), 'Compact quad-mode planar phased array with wideband for 5g mobile terminals', *IEEE Transactions on Antennas and Propagation (In press)* .

Zhang, S., Chen, X., Syrytsin, I. & Pedersen, G. F. (2017), 'A Planar Switchable 3D-Coverage Phased Array Antenna and Its User Effects for 28 GHz Mobile Terminal Applications', *IEEE Transactions on Antennas and Propagation* **65**(12), 6413–6421.